Mon. Not. R. Astron. Soc. **296,** 564–568 (1998)

Spectrophotometry of the planetary nebula KjPn 8

R. Vázquez,[1,2] R. L. Kingsburgh[2,3] and J. A. López[2]

[1] *Instituto de Astrofísica de Andalucía, CSIC, Apdo. Postal 3004, 18080 Granada, Spain*
[2] *Instituto de Astronomía, UNAM, Apdo. Postal 877, 22800 Ensenada, B. C., Mexico*
[3] *Department of Physics and Astronomy, York University, 4700 Keele Street, North York, Ontario, Canada M3J1P3*

Accepted 1997 November 28. Received 1997 November 26; in original form 1997 September 8

ABSTRACT

Flux-calibrated low-resolution spectra covering the optical wavelength range from 3400 to 7500 Å have been obtained over the central region and the surroundings of the extraordinary planetary nebula (PN) KjPn 8 (PNG 112.5-00.1). The spectrum from the core is of low excitation with T_e(N II) = 8000 K and n_e(S II) = 550 cm^{-3}. KjPn 8 is found to be a Type I PN according to the original classification scheme of Peimbert & Torres-Peimbert, with enriched He/H and N/O ratios with respect to mean values for PN. Increased O/H, Ne/H and Ar/H ratios over those of average PN reflect the possible metal-rich environment from which the progenitor star formed, and also are similar to those found in the extreme Type I PN He 2-111. The N/H ratio is found to be only moderately high compared to the average PN and consequently, the large O abundance pulls the N/O ratio towards the lower limit of the criterion for Type I planetary nebulae (PNe) in this case. In addition, the spectra of some knots and faint regions in the KjPn 8 surroundings are presented, which show only a few spectral lines. Low electron densities ranging from 100 to 300 cm^{-3} have been derived in these outer regions.

Key words: ISM: abundances – planetary nebulae: individual: KjPn 8.

1 INTRODUCTION

KjPn 8 (K 3-89, PK 112-00 1, PNG 112.5-00.1) is a remarkable planetary nebula (PN) in many ways. The huge (14×4 arcmin^2) envelope surrounding the otherwise innocuous compact core (López, Vázquez & Rodríguez 1995, hereafter LVR95) place it as the bipolar PN with the largest angular extent known to date, which may only indicate its proximity. Furthermore, LVR95 discovered a bipolar rotating episodic jet (BRET) in this object, with symmetric pairs of groups of knots oriented at different position angles within its extensive bipolar halo. These knots were found to be bright in low-excitation species, such as [N II], [O II] and [S II]. In addition, line fluxes presented by LVR95 were indicative of the presence of substantial collisional ionization in these knots. Subsequently, López et al. (1997, hereafter LMBR97) found direct kinematic evidence of the action of this BRET. High-velocity outflows with speeds of $\simeq$320 km s^{-1} and angled at $\simeq 30^\circ$ to the plane of the sky were found to be responsible for the formation of the diametrically opposed groups of knots originating as the episodic jet ploughs into the walls of the bipolar cavity. A general discussion on collimated outflows in planetary nebulae (PNe), including BRETs, is presented by López (1997).

The core of KjPn 8 was classified as a PN by Kazarian & Parsamian (1971) and it has been considered as a true PN by Kohoutek (1972), Sabbadin (1986) and Acker et al. (1992). The core has also been listed as a helium-enriched PN by Kaler et al. (1996). LMBR97 found from 3.5-cm and 6-cm radio continuum VLA observations a thermal spectral index in the core, with the radio maps revealing a clumpy structure. Recently, Huggins et al. (1997) have reported detection of CO emission surrounding the KjPn 8 core, originating in an expanding disc the axis of which is aligned with the most recent bipolar outflows and with typical young PNe/AGB star spectral line profiles.

The extraordinary characteristics of this object have driven us to explore further the physical conditions in its nebular core and the large structure of its surroundings. The results presented here contain an improved reanalysis of the KjPn 8 spectra presented by LVR95.

2 OBSERVATIONS

The low-dispersion spectroscopy was obtained with a Boller & Chivens spectrometer at the f/7.5 focus of the 2.1-m San Pedro Mártir OAN-UNAM telescope on 1994 December 2. A 300 line mm^{-1} grating was used with a Tektronix 1024×1024 pixel CCD (24-μm square pixels) as the detector. The wavelength interval covers from 3400–7500 Å, with 9-Å spectral resolution, as judged by the FWHM of the comparison arc lines. A 220 μm (= 2.9 arcsec) slit width was used. Exposure times for these spectra were 1200 and 1800 s. In addition, a wide slit spectrum (660 μm) with an exposure time of 600 s was taken in order to obtain the integrated Hβ emission from the core. Table 1 shows the log of the observations and the region along the slit where each 2D image was co-added in order to extract the integrated spectrum. Fig. 1 presents

Table 1. Log of observations. Regions with the same PA and exposure time are extracted from the same slit position.

Region	Position angle (°)	Exposure time (sec)	Slit width (μm)	Slit length (arcsec)
A1	45	1800	220	15.6
B1	45	1800	220	17.4
C1	105	1800	220	3.0
A3	114	1200	220	5.4
core	114	1200	220	4.8
core (wide)	114	600	600	4.2
D1	166	1800	220	3.6
D2	166	1800	220	7.8

the slit positions superimposed on an Hα image taken from LVR95. The knots are labelled as in LVR95, with two knots D1 and D2 added here.

The spectral images were trimmed, bias-substracted and flat-fielded with standard techniques using IRAF. Flux calibration was performed using sensitivity functions derived from four different standard stars, HD 217086, Hiltner 102, Hiltner 600 and Feige 34, with self-consistent results. In Fig. 2 the final calibrated core spectrum is shown at two different scales; the top panel shows the full flux range, and the bottom panel highlights the less intense spectral lines. This calibrated spectrum has been extracted from the co-addition of 4.8 arcsec along the slit, centered on the KjPn 8 core with the slit located at PA 114°.

The spectra presented in LVR95 had a poor background substraction, so there are some discrepancies with line fluxes presented here and in that paper. The [O I] λ6300 and λ6365 features were predominantly a result of the night sky, and show the greatest discrepancy. In addition, the long-slit spectral images contain diffuse extended emission throughout the length of the slit, which is likely to originate mainly from the envelope surrounding the core. The weakest lines in the blue region of the spectrum (λλ3868, 3968, Hδ) were most greatly affected by the background substraction, and also show a great discrepancy with the fluxes presented in LVR95 (up to 50 per cent). The remaining lines agree with the corresponding values from LVR95, according with their uncertainty (10 per cent).

3 RESULTS AND DISCUSSION

3.1 Reddening

A logarithmic nebular extinction coefficient $c(\mathrm{H}\beta) = 0.71$ has been derived for the core from the Balmer Hα/Hβ ratio. Case B (Baker & Menzel 1938) for radiative recombination was assumed, adopting $\mathrm{H}\alpha/\mathrm{H}\beta = 2.847$ (for $T_e = 10^4$ K and $n_e = 10^4$ cm^{-3}; Hummer & Storey 1987). The difference between this value for $c(\mathrm{H}\beta)$ to that derived by LVR95 ($c(\mathrm{H}\beta) = 0.75$) is related to the improved background subtraction in the present work. For comparison, Acker et al. (1991) derive a value of $c(\mathrm{H}\beta) = 0.65$, whereas Kaler et al. (1996)

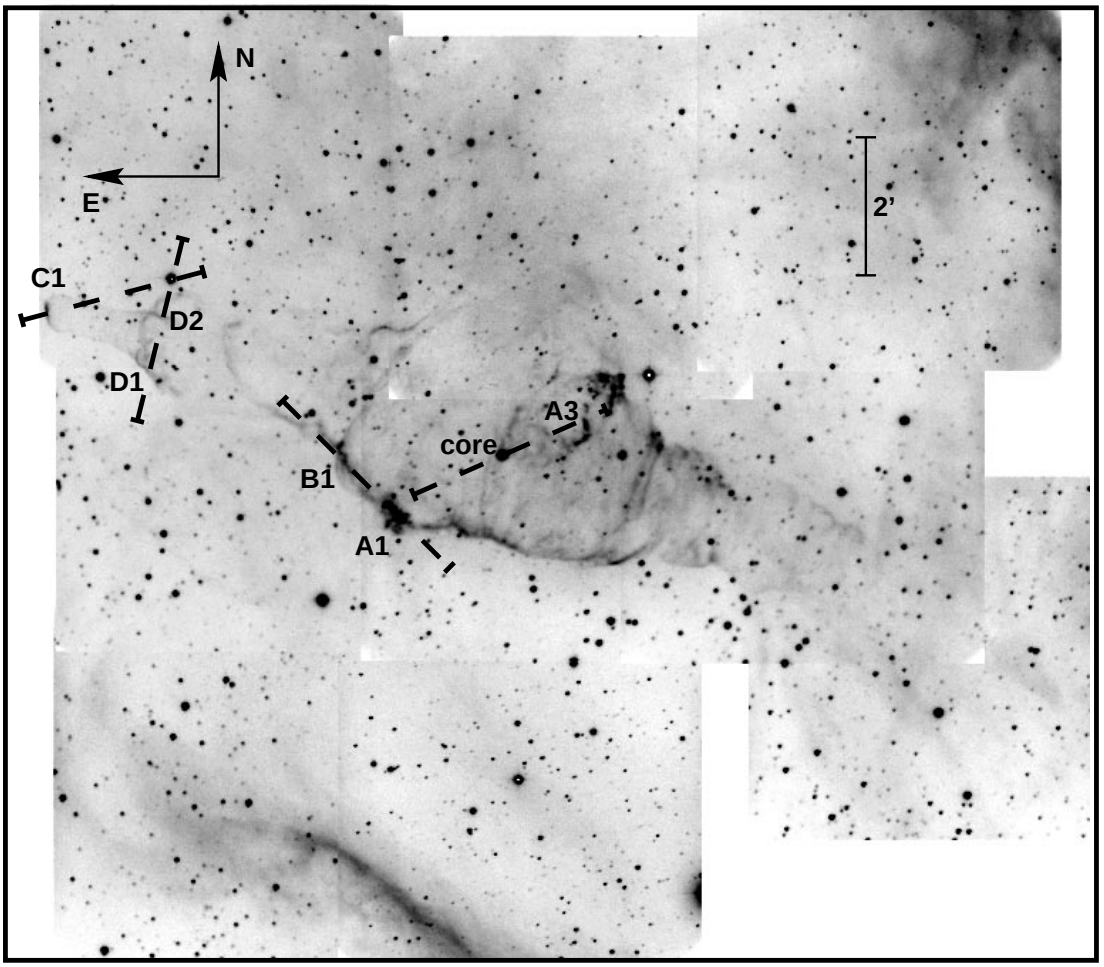

Figure 1. Hα CCD mosaic of KjPn 8, taken from LVR95. Slit positions and particular regions discussed in the paper are indicated.

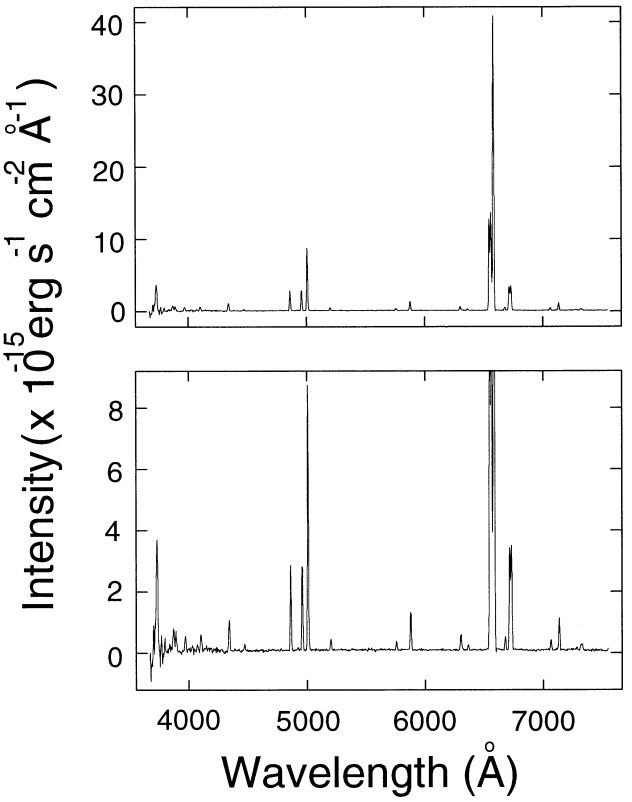

Figure 2. The optical spectrum from the core of KjPn 8. Top: full scale. Bottom: expanded scale highlighting weaker emission lines.

report a $c(\mathrm{H}\beta) = 0.90$ from their large aperture observations (8-arcsec diameter).

Table 2 presents the observed and dereddened fluxes for the core spectrum, where $\log F_{\mathrm{H}\beta} = -13.4$ (with $F_{\mathrm{H}\beta}$ in erg cm^{-2} s^{-1}). The Galactic reddening law of Howarth (1983), (f_λ) has been used.

3.2 Physical parameters of the core

As the [O III] λ4363 emission line is only very weakly present in the core spectrum, the [O III] electron temperature was not derived. The [N II] electron temperature is more appropriate to use for deriving ionic abundances for KjPn 8, as it is a low ionization nebula. The $I(\lambda6548 + \lambda6584)/I(\lambda5755)$ line ratio yields $T_\mathrm{e} = 8000$ K, which was adopted in the calculation of the ionic abundances. The [S II] line ratio $I(\lambda6717)/I(\lambda6731)$ was used to estimate the electron density, yielding $n_\mathrm{e} = 550\,\mathrm{cm}^{-3}$. The electron temperature and density were derived using the EQUIB code (written by I. D. Howarth and modified by S. Adams, 1981–1984) solving the statistical equilibrium equations iteratively to calculate n_e as a function of T_e for each ratio.

The ionized mass in the compact core can also be estimated from the wide-slit Hβ flux. Assuming a filling factor $\epsilon = 0.75$, a distance of 1 kpc (LVR95) and following Gathier (1987), the value for the ionized mass is $M_\mathrm{i} = 3 \times 10^{-4} \mathrm{M}_\odot$. This value coincides within a factor of 2 with the estimate of Huggins et al. (1997), who also adopted the same distance.

3.3 Ionic abundances of the core

Ionic abundances have been derived using the EQUIB code and the dereddened relative fluxes of the corresponding emission lines.

Table 2. Observed (F_λ) and dereddened (I_λ) fluxes for the core relative to $F_{\mathrm{H}\beta} = 100$ and $I_{\mathrm{H}\beta} = 100$. A colon indicates an uncertainty of approximately 50 per cent.

Ion	λ_0(Å)	f_λ	F_λ	I_λ
[O II]	3727	0.257	187	285
[Ne III]	3868	0.231	31.1	45.3
[Ne III]	3969	0.211	21.2	29.9
Hδ	4101	0.182	25.6	34.4
Hγ	4340	0.127	40.6	49.9
He I	4471	0.096	7.1:	8.3:
Hβ	4861	0.000	100	100
He I	4925	–0.016	3.5:	3.4
[O I]	4959	–0.024	98.5	94.7
[O I]	5007	–0.036	311	294
[N I]	5198	–0.083	13.7	12.0
[N II]	5755	–0.195	10.4	7.6
He I	5876	–0.215	47.1	33.2
[O I]	6300	–0.282	21.3	13.5
[O I]	6364	–0.291	6.3	3.9
[N II]	6548	–0.318	485	289
Hα	6563	–0.320	480	285
[N II]	6583	–0.323	1519	897
He I	6678	–0.336	16.1	9.3
[S II]	6716	–0.342	125	71.6
[S II]	6731	–0.344	127	72.3
He I	7065	–0.387	13.6	7.3
[Ar III]	7135	–0.396	36.2	19.0
[O II]	7327	–0.418	12.8	6.4

The $\mathrm{He}^+/\mathrm{H}^+$ abundance was derived from the standard relation

$$\frac{n(\mathrm{He}^+)}{n(\mathrm{H}^+)} = \frac{I_\lambda}{I_{\mathrm{H}\beta}} \frac{\alpha_{\mathrm{eff}}^{\mathrm{H}\beta}}{\alpha_{\mathrm{eff}}^{\mathrm{He}^+}} \frac{\lambda}{4861} (1 + CR_\lambda)^{-1}$$

where the effective recombination coefficients α_{eff} are functions of temperature and density, and they were taken from Hummer & Storey (1987, Hβ) and from Brocklehurst (1971, He^+). The $(1 + CR_\lambda)^{-1}$ factor corrects for collisional effects (Clegg 1987). The results obtained from the He I λ5876 and λ6678 spectral lines are listed in Table 3 together with the ionic abundances by number for the other elements observed.

Elemental abundances have been derived from the data in Table 3 combined with the ionization correction factors (ICF) from Kingsburgh & Barlow (1994, hereafter KB94). The results are presented in Table 4. For comparison, this table also contains the representative mean abundances for normal and Type I PNe from KB94, Galactic H II regions (Dufour 1984), the Sun (Grevesse & Anders 1989) and the peculiar Type I PN He 2-111 (an extreme case of helium overabundance). Note that the abundance analysis presented here does not attempt to estimate the contributions by neutral ions. As KjPn8 is a low excitation object, and lines of [O I] and [N I] are seen in the spectra, neutral material would be present, but is assumed to be in the same ratio as neutral hydrogen. Also, uncertainties in the ionization correction factors owing to KjPn 8 being of low ionization are discussed below.

3.3.1 Helium

The He/H ratio for KjPn 8 is 0.229 (Table 4) and is a factor of 2 higher than the 'average' PNe and H II regions, also being comparable to the extreme Type I PNe He 2-111, where He/H = 0.219. Such large He/H ratios in nebulae have yet to be predicted accurately by theory.

Table 3. Ionic abundances by number.

Ion	λ_0 (Å)	$A(x)$
He^+/H^+	5876	0.231
	6678	0.227
	Average	0.229
O^+/H^+	3726+29	6.68×10^{-4}
O^{+2}/H^+	4959	2.31×10^{-4}
	5007	2.49×10^{-4}
	Average	2.40×10^{-4}
N^+/H^+	6548	3.10×10^{-4}
	6583	3.27×10^{-4}
	Average	3.18×10^{-4}
S^+/H^+	6717	6.73×10^{-6}
	6731	6.72×10^{-6}
	Average	6.72×10^{-6}
Ne^{+2}/H^+	3868	1.25×10^{-4}
Ar^{+2}/H^+	7135	2.81×10^{-6}
$O^+ + O^{+2}/H^+$		9.08×10^{-4}
N^+/O^+		4.76×10^{-1}
S^+/O^+		1.01×10^{-2}
Ne^{+2}/O^{+2}		5.21×10^{-1}

3.3.2 *Oxygen*

The O/H ratio is a factor of 1.9 higher than the 'average' non-Type I and Type I PN, and comparable to the solar oxygen abundance, although is within the range of O/H ratios seen in the KB94 sample. Use of the [O III] electron temperature in the O^{2+} zone would decrease the overall abundance somewhat, although the bulk of O is in the O^+ stage of ionization, where T_e(N II) is most appropriate. The largest uncertainty in the oxygen abundance lies in the uncertainty in reddening, and the [O II] λ3727 flux is strongly sensitive to this. The high value for O/H is likely to be real, and a result of the location of the object in the Galactic plane (at $b = 0$).

3.3.3 *Nitrogen*

Type I PNe are defined as objects whose abundances satisfy the conditions $\log N/O \geq -0.3$ and $He/H \geq 0.125$, according to the scheme of Peimbert & Torres-Peimbert (1983). KB94 revised this scheme, and stated that for the Type I PN, nitrogen enrichment is seen via CN cycle burning of primary carbon in the 3rd dredge-up. Their criterion for Galactic Type I PN was log N/O>−0.10, based on the fact that the total nitrogen abundance had to exceed the total C+N abundance present when the progenitor star formed. KjPn 8 has log N/O= −0.3, which does not satisfy the KB94 criterion, although the N/H ratio is 4.32×10^{-4}, a factor of 3.1 over the 'average' non-Type I PN. It is possible, that, owing to the location in the Galactic plane, the progenitor star for KjPn 8 had a high N abundance. In general, relative abundances to oxygen are preferred, to look at enrichment resulting from stellar evolution and nucleosynthesis without worrying about enrichment owing to Galactic chemical evolution. The N/O ratio for KjPn 8 is enriched a factor of 1.7 over the 'average' PN, so it is enriched in nitrogen, and classified as a Type I PN according to Peimbert & Torres-Peimbert (1983), but not KB94.

3.3.4 *Neon*

We have derived a high Ne/O ratio of 0.52 for KjPn 8, compared to the average Ne/O = 0.26. The value lies ∼0.5 dex above the O–Ne trend seen by Henry (1989), in the sense that KjPn 8 is overly rich in Ne compared to O. Our total Ne abundance is somewhat uncertain, as it is derived using a high ICF (3.83), based on the O/O^{2+} ratio. This ICF is more appropriate for higher excitation objects and generally corrects for higher stages of ionization, and may overestimate the Ne^+ contribution. Another problem may be that the assumed T_e(N II) may be too low for the Ne^{2+} zone, thus overestimating the Ne^{2+} abundance. The Ne/O ratio however, does agree with Ne/O = 0.50 derived for He 2-111 (KB94), and is the highest seen in PN. In the case of He 2-111, Ne is spread throughout the 2+, 3+ and 4+ stages of ionization, and the Ne/O ratio does not have the same uncertainty associated with KjPn 8. It would be worthwhile to try to observe directly the Ne^+ stage of ionization with other lines, and also the [Ne III] 15.5-μm line to derive the T_e appropriate for the Ne^{2+} zone.

3.3.5 *Argon and sulphur*

The Ar/O ratio for KjPn 8 is equivalent to that seen in non-Type I and Type I PN, within the errors. In the case of sulphur, the ICF scheme of KB94 is not appropriate for such a low-ionization object. Here we have assumed that since S^+ is the dominant stage of ionization, $S/H = S^+/H^+$. This in fact would be a lower limit, and the S/O ratio is a factor of ∼2 lower than the average values for non-Type I and Type I PN.

3.4 The knots and faint regions

Observed fluxes from the knots and faint regions in the extended envelope are presented in Table 5. Dashes are used to indicate that either the corresponding spectral line was not observed or that it had a too low signal-to-noise ratio to be reliably measured. Electron densities from the [S II] λ6717/λ6731 ratio were estimated assuming an electron temperature of $T_e = 8000$ K, with resulting values ranging from 100 to 300 cm^{-3}.

Table 4. Comparison of elemental abundances by number.

Ion	[a]ICF	KjPn 8	[b,c]He 2-111	[b]PNe mean	[b]Type I PNe mean	[d]H II regions mean	[e]Solar
He/H	—	0.229	0.219	0.112	0.129	0.100	0.098
O/H	—	8.96	8.45	8.69	8.65	8.70	8.93
N/H	1.36	8.64	8.85	8.14	8.72	7.57	8.00
Ne/H	3.79	8.68	8.15	8.10	8.09	7.90	8.09
Ar/H	1.87	6.72	6.63	6.38	6.42	6.42	—
S/H	1.00	>6.83	7.20	6.91	6.91	7.06	7.24

Notes to table. All values are given in logarithmic scale with H=12, with the exception of He/H. [a]Ionization correction factors from Kingsburgh & Barlow (1994). [b]Kingsburgh & Barlow (1994). [c]PA = 60°, slit: 1.0 arcsec. [d]Dufour (1984). [e]Grevesse & Anders (1989).

Table 5. Observed fluxes from the knots and faint regions in the envelope of KjPn 8 relative to $F_{H\beta}$ = 100, nebular extinction coefficients and electron densities. A colon indicates an uncertainty of approximately 50 per cent; a double colon indicates an uncertainty greater than 50 per cent.

Ion	λ_0 (Å)	A1	A3	B1	C1	D1	D2
[O II]	3727	442:	—	327:	—	—	—
[Ne III]	3868	—	—	54.7:	—	—	—
Hγ	4340	44.2:	—	—	—	—	—
Hβ	4861	100	100:	100	100::	100::	100::
[O III]	4959	48.1:	—	—	—	—	—
[O III]	5007	120	—	—	—	—	—
[N I]	5198	81.2	63.3:	38.8:	—	—	—
[N II]	5755	—	133:	286	—	116	—
He I	5876	—	—	89.6	—	—	—
[O I]	6300	138	243	197	—	98.0	96.6
[O I]	6364	52.6	—	59.9	—	35.6:	—
[N II]	6548	528	73.4:	69.8	127:	143:	99.1:
Hα	6563	855	579	430	1986	688	1099
[N II]	6583	1598	253	210	481	355	324
[S II]	6716	548	503	212	486	322	—
[S II]	6731	410	403	159	437	252	—
$c(H\beta)$		1.49	0.96	0.56	2.64	1.20	1.83
n_e(S II)		100	200	100	300	150	—

The shock nature of the emission from these knots was deduced from the diagnostic diagram presented by LVR95 (their fig. 4), where the knots occupy the region corresponding to collisional excitation. The new values of the line intensity ratios do not affect significantly their location in this diagram. LMBR97 measured very high velocities in these knots that support the likely shock nature of their emission. We have compared the observed line intensities with the theoretical models by Hartigan, Raymond & Hartmann (1987) and Dopita & Sutherland (1995); however, the steep Balmer decrement observed in these regions could not be consistently matched within these models.

The Hβ fluxes measured from the faint regions C1, D1 and D2 are considered uncertain. The Hβ flux from knot A3 also has an uncertainty of 50 per cent. Thus, observational errors could in principle account for the high Hα/Hβ ratios in these regions. However, the spectrum of knot A1 is of good signal-to-noise ratio, and also shows a high Hα/Hβ ratio. It is possible that these high Hα/Hβ ratios may result from a combination of collisional excitation processes and additional dust mixed within the condensations that form in the knots. Given the uncertainty in both the observations and the interpretation of these spectra, no further analysis has been attempted, and the reddening correction was not applied to these spectra.

3.5 KjPn 8 versus He 2-111

KjPn 8 and He 2-111 are two extreme PNe whose similarities and differences are worth pointing out briefly for future comparisons of this peculiar class of objects. Both are bipolar, with huge angular sizes and extreme radial velocities in their outer shells (LMBR97, Meaburn & Walsh 1989). Both are extreme Type I PNe with very large He/H ratios and also similar Ne/O and Ar/H ratios. He 2-111 is a high-excitation object showing high-ionization species as He II and [Ne V]. KjPn 8 has a low-excitation spectrum. In addition, the N/O ratio in He 2-111 is 2.5, whereas in KjPn 8 is only 0.48.

4 CONCLUSIONS

A spectrophotometric analysis of the optical line emission spectrum of the core of the PN KjPn 8 has been carried out. The spectrum is found to be of low excitation, with $T_e(N\,II) = 8000$ K, and $n_e(S\,II) = 550\,cm^{-3}$. A value of $c(H\beta) = 0.71$ is obtained from the Hα/Hβ ratio. Elemental abundances have been derived and found to correspond to those of extreme Type I PNe, such as He 2-111. The available data on this object indicate a relatively young PN, evolving from a massive progenitor within a previously enriched environment in the Galactic plane.

Spectra were also obtained from additional regions in the nebular envelope, some of them considerably faint and for which the line fluxes have been considered unreliable for an elaborate analysis. For the case of the relatively brighter knots, as A1, the steep Balmer decrement observed could be because of a combination of collisional excitation effects plus mixed dust within these condensations. [S II] electron densities have been estimated for most of these outer locations. The corresponding values, assuming a $T_e = 8000$ K, denote low electron densities ranging from 100 to 300 cm^{-3}.

ACKNOWLEDGMENTS

We wish to thank the staff of the San Pedro Mártir Observatory for their excellent support during these observations. RV is in grateful receipt of a graduate scholarship from the Agencia Española de Cooperación Internacional (Spain) and complementary support from DGAPA-UNAM (Mexico). RV also thanks Drs J. M. Torrelles and L. F. Miranda for helpful comments. JAL acknowledges continuous support from CONACYT and DGAPA-UNAM.

REFERENCES

Acker A., Stenholm B., Tylenda R., Raytchev B., 1991, A&AS, 90, 89
Acker A., Ochsenbein F., Stenholm B., Tylenda R., Marcout J., Schohn C., 1992, Strasbourg–ESO Catalogue of Galactic Planetary Nebulae. ESO, Münich
Baker J. G., Menzel D. H., 1938, ApJ, 88, 52
Brocklehurst M., 1971, MNRAS, 153, 471
Clegg R. E. S., 1987, MNRAS, 229, 31P
Dopita M. A., Sutherland R. S., 1995, ApJ, 455, 468
Dufour R. J., 1984, in van der Bergh S., de Boer K. S., eds, Proc. IAU Symp. 108, Structure and Evolution of the Magellanic Clouds. Kluwer, Dordrecht, p. 353
Gathier R., 1987, A&AS, 71, 245
Grevesse N., Anders E., 1989, in Waddington C. J., ed., AIP Conf. Proc. 183, Cosmic Abundances of Matter. Am. Inst. Phys., New York, p. 1
Hartigan P., Raymond J., Hartmann L., 1987, ApJ, 316, 323
Henry R. B. C., 1989, MNRAS, 241, 453
Howarth I. D., 1983, MNRAS, 203, 301
Huggins P. J., Bachiller R., Cox P., Forveille T., 1997, ApJ, 483, L57
Hummer D. G., Storey P. J., 1987, MNRAS, 224, 801
Kaler J. B., Kwitter K. B., Shaw R. A., Browning L., 1996, PASP, 108, 980
Kazarian M. A., Parsamian E. S. P., 1971, Astron. Tsirk., 602, 6
Kingsburgh R. L., Barlow M. J., 1994, MNRAS, 271, 257 (KB94)
Kohoutek L., 1972, A&A, 16, 291
López J. A., 1997, in Habing H., Lamers H., eds, Proc. IAU Symp. 180, Planetary Nebulae. Kluwer, Dordrecht, p. 197
López J. A., Vázquez R., Rodríguez L. F., 1995, ApJ, 455, L63 (LVR95)
López J. A., Meaburn J., Bryce M., Rodríguez L. F., 1997, ApJ, 475, 705 (LMBR97)
Meaburn J., Walsh J. R., 1989, A&A, 223, 277
Peimbert M., Torres-Peimbert S., 1983, in Flower D. R., ed., Proc. IAU Symp. 103, Planetary Nebulae. Reidel, Dordrecht, p. 233
Sabbadin F., 1986, A&AS, 65, 301
This paper has been typeset from a TEX/LATEX file prepared by the author.